Self-Activated Transparent All-Graphene Gas Sensor with Endurance to Humidity and Mechanical Bending

Yeon Hoo Kim,[†] Sang Jin Kim,[‡,#] Yong-Jin Kim,[‡,§] Yeong-Seok Shim,[†] Soo Young Kim,[⊥] Byung Hee Hong,[*,‡] and Ho Won Jang[*,†]

[†]Department of Materials Science and Engineering, Seoul National University, Seoul 151-744, Republic of Korea, [‡]Department of Chemistry, Seoul National University, Seoul 151-742, Republic of Korea, [§]School of Physics and Astronomy, University of Manchester, Oxford Road, Manchester M13 9PL, United Kingdom, and [⊥]School of Chemical Engineering and Materials Science, Chung-Ang University, Seoul 156-756, Republic of Korea. [#]Present address: Institute of Advanced Composite Materials, Korea Institute of Science and Technology, Eunha-ri san 101, Bongdong-eup, Wanju-gun, Jeonbuk 565-905, Republic of Korea.

ABSTRACT Graphene is considered as one of leading candidates for gas sensor applications in the Internet of Things owing to its unique properties such as high sensitivity to gas adsorption, transparency, and flexibility. We present self-activated operation of all graphene gas sensors with high transparency and flexibility. The all-graphene gas sensors which consist of graphene for both sensor electrodes and active sensing area exhibit highly sensitive, selective, and reversible responses to NO_2 without external heating. The sensors show reliable operation under high humidity conditions and bending strain. In addition to these remarkable device performances, the significantly facile fabrication process enlarges the potential of the all-graphene gas sensors for use in the Internet of Things and wearable electronics.

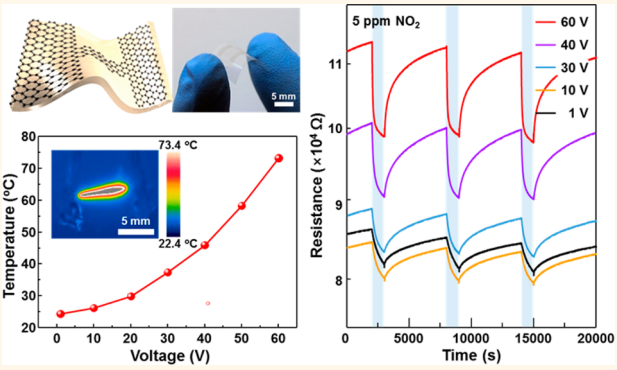

KEYWORDS: graphene · gas sensors · self-activation · Internet of Things · wearable devices

Internet of things (IoT) refers to the interconnected network of physical objects that contain embedded technology to exchange information or processed data with operators, manufacturers, or other connected devices.[1] One of the most important components of the IoT is sensors, as they offer massive information about the internal states of the objects and the external environment.[2] Gas sensors that transmit information about the presence and the concentration of a particular gas in ambient atmosphere have attracted enormous attention as keys to innovations in the fields of comfort, security, health, environment, and energy savings.[3−6] Gas sensors required by the IoT should meet special requirements such as low power consumption, low cost, small size, and easy integration into existing technologies.[7] Among various types of gas sensors, chemoresistive gas sensors based on semiconducting materials have been considered as suitable candidates for the IoT due to low cost and small size.[7−10] Gas sensors based on nanostructured semiconducting metal oxides lead to high responses to various gases, but they operate with external heaters to maintain the materials at elevated temperatures.[7,11] The use of an external heater not only increases the power consumption but also causes thermal safety problems, hindering practical applications for the IoT.

Graphene, a two-dimensional (2D) carbon monolayer crystal, is considered as a candidate material for the next-generation high-performance gas sensors operating at room temperature, since the surface without bulk is highly sensitive to the adsorption and desorption of gaseous molecules.[12−20] However, the main drawback of graphene-based sensors is their extremely sluggish response and incomplete recovery to the initial state after a sensing event, thus making the sensors incapable of producing repeatable sensing signals even upon exposure to

* Address correspondence to byunghee@snu.ac.kr, hwjang@snu.ac.kr.

Received for review July 28, 2015 and accepted August 30, 2015.

Published online August 30, 2015
10.1021/acsnano.5b04680

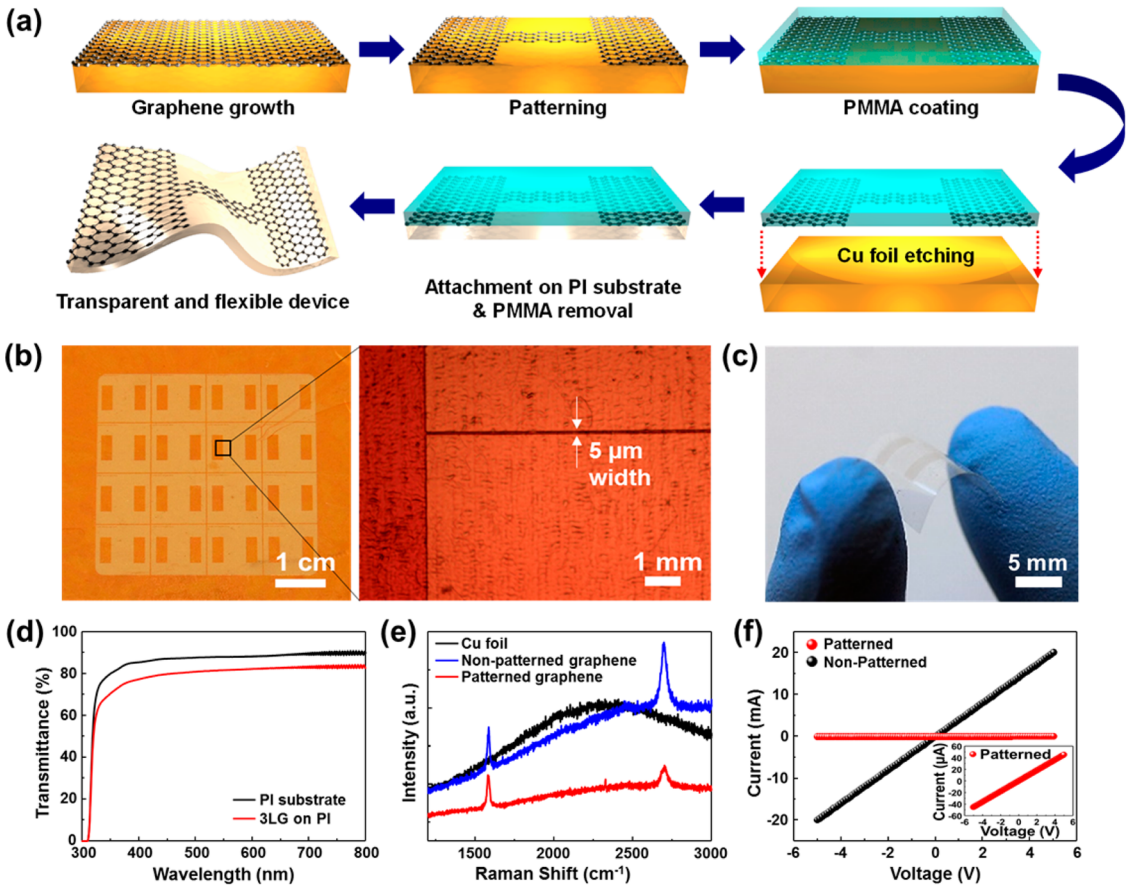

Figure 1. (a) Fabrication procedure of an all-graphene sensor. (b) Optical microscopic images of patterned graphene on a Cu foil. (c) Photograph of a fabricated all-graphene gas sensor on a PI substrate. (d) UV−vis transmittance spectra of PI substrate and final device. (e) Raman spectra of a Cu foil and graphene on the Cu foil before and after patterning. (f) Current−voltage characteristics of nonpatterned and patterned all graphene sensors.

the same analyte concentration at room temperature.[13,16,21−23] The long response and recovery time of the graphene-based sensors originates from the slow process of NO_2 adsorption on the graphene surface at room temperature.[24,25] Fowler *et al.*[16] showed that a gas sensor based on reduced graphene oxide required an elevated operation temperature of 149 °C for reversible sensor response and recovery. In addition to the sensing material itself, stable contact between graphene and sensor electrodes is also required for reliable sensor operation. When chemical vapor deposited graphene is transferred to sensor electrodes or reduced graphene oxide flakes are drop-casted on sensor electrodes, weak binding between graphene and noble metals such as Pt and Au can be the origin of low signal-to-noise ratios in graphene-based gas sensors. To fulfill these requirements, the development of self-activated gas sensors consisting of only graphene for both active area and sensor electrodes is vital.

Here, we report self-activated all-graphene gas sensors that can detect NO_2 reversibly without external heating. The sensing properties of the all-graphene gas sensors are significantly enhanced by self-activation, Joule heating in a micropatterned graphene channel that depends on sensor geometry, and applied bias voltage. The self-activation is clarified by infrared imaging and comparison with external heating. The voltage dependence of sensor response to NO_2 is presented. We also present the linearity between NO_2 concentration and the sensor response and the high selectivity of the sensor response to NO_2. As both active sensing area and sensor electrodes consist of only graphene, the fabrication process is quite simple and the sensors fabricated on polyimide (PI) substrate are entirely transparent and highly flexible.

RESULTS AND DISCUSSION

Three-layer graphene (3LG) was grown on a Cu foil using a chemical vapor deposition (CVD) method. The 3LG was patterned directly on the Cu foil because of difficulties in patterning on a flexible polymer substrate. Poly(methyl methacrylate) (PMMA) was coated on top of the patterned graphene to transfer the sample on a target substrate. The Cu foil was etched using $FeCl_3$, and the patterned graphene with PMMA was transferred on a PI substrate (Figure 1a). The PI substrate was employed since it is transparent, flexible, and thermally more stable than other polymer substrates. The key

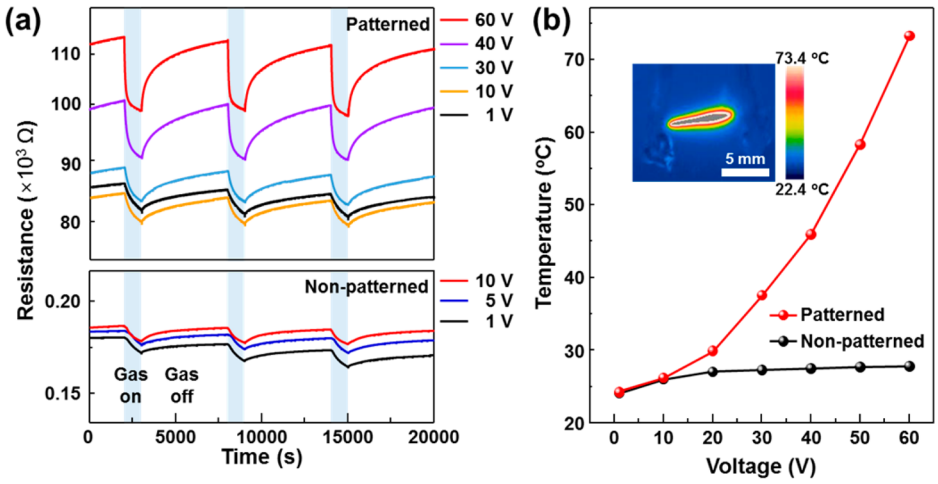

Figure 2. (a) Response curves of patterned and nonpatterned graphene sensors to three pulses of 5 ppm of NO_2. (b) Thermographic image and thermal characteristics with different bias voltages.

idea of this work is inducing current crowding in the micropatterned narrow electrical channel of 3LG on the transparent and flexible substrate, resulting in the self-activation. Such a self-activation in the narrow graphene channel is analogous to Joule heating in typical platinum-based micro heaters. Figure 1b shows optical microscopic images of patterned graphene with the narrow electrical channel of 5 μm width and 5 mm length on a Cu foil. The width of the channel was limited to 5 μm because the channels under 5 μm could not be made reproducibly in our technique.

The final devices are entirely transparent and flexible as shown in the photograph of a final sensor device on a PI substrate in Figure 1c, which has not been achieved yet since typical sensors contain nontransparent and nonflexible parts such as sensor electrodes or heaters.[26,27] The transmittance spectra of a PI substrate and the substrate with 3LG over the wavelength range of 300−800 nm are shown in Figure 1d. The transmittance of the PI substrate and the substrate at 550 nm with 3LG is ∼88% and ∼80%, respectively. Owing to this high transmittance, the fabricated sensors are barely visible, suggesting that the sensors can be applied to next-generation transparent electronics. The as-grown (nonpatterned) and patterned 3LG was characterized by Raman spectroscopy. The absence of a measurable D-band in Figure 1e denotes the low-defect density of the 3LG.[28] Since low-energy binding sites, like the carbon sp^2 bonds, result in a fast gas reaction and high-energy binding sites such as point defects offer a slow gas reaction, superior sensing performance of our device is expected by the absence of a D-band.[29] As the sensors are composed of only graphene, there is no heterogeneous junction between sensor electrodes and active sensing layer so that the both patterned (5 μm × 5 mm sensing area) and nonpatterned (1 cm × 1 cm sensing area) sensors display linear current−voltage (I−V) characteristics as shown in Figure 1f. Such an Ohmic behavior is very important for reliable sensor performance because resistance changes in the active region can be exactly measured without attenuation. The similar resistances of 10 patterned sensors indicate the reproducibility of the fabrication procedure (Supplementary Figure S1). The length of the patterned graphene channel was fixed at 5 mm, which is moderate for making the sensor resistance appropriate for chemoresistive gas sensing.

Figure 2a shows dynamic sensing transients of the patterned and nonpatterned all-graphene sensors. The devices were exposed to three consecutive pulses of 5 ppm of NO_2 balanced with dry air. The patterned graphene sensor shows a dramatic enhancement in response with increasing the bias voltage. Since the interval time between each exposure is not enough for full recovery, the base resistance is slightly shifted for multiple exposures. The response of the patterned graphene sensor (defined here as $(R_{gas} - R_{air})/R_{air} \times 100$, where R_{air} and R_{gas} denote the resistance of the sensor in dry air and the resistance of the sensor by exposure to the test gas) is 4.47% at 1 V and 12.49% at 60 V. In the previous works,[12,21,30−33] the graphene-based gas sensors showed responsees of ∼5% to 1−20 ppm of NO_2 at room temperature, while our device exhibits a response of ∼12% to 5 ppm of NO_2. With increasing the bias voltage, the sensor also shows improved response and recovery (Supplementary Figure S2a,b). For the nonpatterned sensor, measurements were only available with the bias voltage under 10 V due to the power limit of the source measurement unit (Keithley 2635B), and the response to 5 ppm of NO_2 is not enhanced by applying 10 V. The response of the nonpatterned sensor is 4.67% and 4.35% at 1 and 10 V, respectively. The nonpatterned sensor shows a larger deviation of the responses than that of the patterned graphene sensor to the consecutive three time pulses of 5 ppm of NO_2 (Supplementary Figure S2c). In contrast, the deviation of continuative responses to 5 ppm of NO_2 was relatively small for the patterned

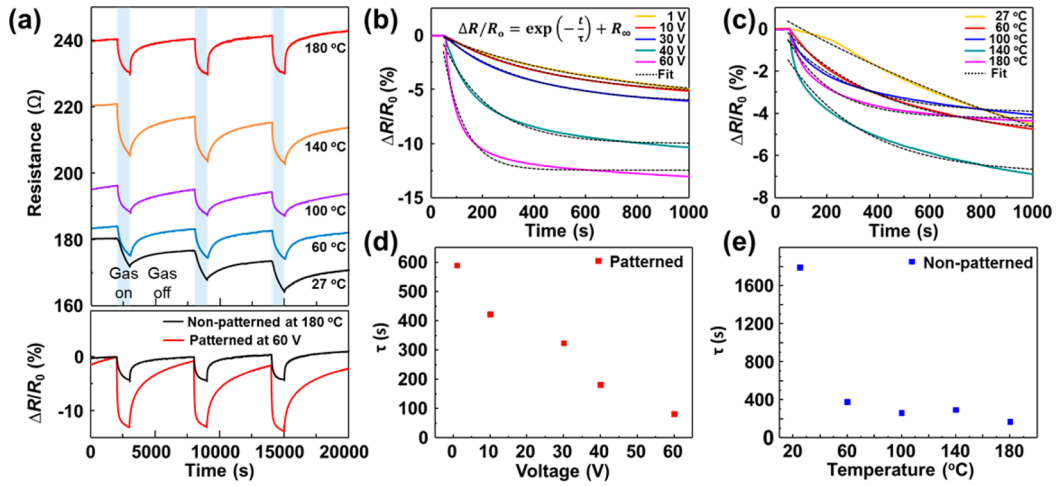

Figure 3. (a) Response curves of the nonpatterned sensor to three pulses of 5 ppm of NO_2 at different temperatures (top) and comparison of the response curve at 180 °C with that of the patterned sensor at 60 V (bottom). (b) Normalized response curves with fits to the exponential decay formula for the patterned and (c) nonpatterned sensors. (d) Decay time, τ, as functions of applied bias voltage for the patterned sensor and (e) temperature for the nonpatterned sensor.

sensor. Because the patterned sensor reached the resistances very close to the original baseline value after each exposure to NO_2, the patterned sensor could have the smaller deviation in the responses compared with that for the nonpatterned sensor. This reliable and repeatable sensing performance of the patterned sensor holds promise in practical applications. For the patterned sensor, response and recovery time (response t_{50} and recovery t_{50} are the time for the sensor's resistance to reach 50% of its steady state value in the gas response and the recovery to original state, respectively) were calculated at each applied voltage. By increasing the bias voltage from 1 to 60 V, the response t_{50} decreased from 328 to 89 s and the recovery t_{50} decreased from 1941 to 579 s (Supplementary Figure S2d).

It is noteworthy that the baseline sensor resistances increase for both the patterned and nonpatterned sensors when the applied voltage is increased from 1 to 60 V. One relevant scenario to explain this result is that the temperature of the active regions in the sensors increases with increasing the bias voltage. Since graphene is metallic, the resistance of the material increases with increasing temperature, which is an indirect evidence of self-activation in the sensors. To confirm the voltage-dependent self-activation, thermographic images of the sensors were obtained with an infrared camera (FLIR SC660). The temperature of the active region in the patterned sensor was measured to 73.4 °C at the applied bias voltage of 60 V (ODA Technologies EX200-6). On the contrary, the temperature of the nonpatterned sensor stays below 30 °C even at 60 V (Figure 2b). In the previous work, graphene-based gas sensors required a minimum temperature of 149 °C for the fast response and full recovery.[16] However, in this work, the fast response and full recovery of the patterned graphene sensor were observed at the relatively low temperature of 73.4 °C. We presumed that the actual temperature on locally heated spots would be higher than the apparent temperature of 73.4 °C. Hence, additional experiments were conducted to prove the presumption.

The response of the nonpatterned graphene sensor to 5 ppm of NO_2 was measured at various temperatures from 27 to 180 °C with a constant applied voltage of 1 V (Figure 3a). The sensor resistance increases to ~240 Ω with increasing temperatures as shown in the patterned graphene sensor with increasing bias voltage. As the temperature increases, the sensor shows faster response and improved recovery. The nonpatterned sensor exhibits full recovery to the original state at 180 °C. However, the response time of the nonpatterned sensor at 180 °C looks still longer than that of the patterned sensor operating at 60 V. To clarify this, the response curves of the patterned and nonpatterned sensors were fit by the exponential decay formula, $\Delta R/R_0\,(t) = \exp(-t/\tau) + R_\infty$, where τ is the time constant and R_∞ the steady-state resistance, as shown in Figures 3b,c. For each fit curve, we extracted the τ value and plotted the τ values as a function of the applied bias voltage for the pattern sensor (Figure 3d) and temperature for the nonpatterned sensor (Figure 3e). The τ value gradually decreases with the voltage for the pattered sensor, while it exponentially decreases with temperature for the nonpatterned sensor. However, the τ value of the patterned sensor with 60 V (82 s) is still lower than that of the nonpatterned sensor at 180 °C (168 s). From this result, it is suggested that imperceptible heating over 180 °C occurred at local spots on the patterned graphene sensor by applying 60 V. We believe that the local heating spots are invisible within the resolution of the infrared camera. Recently, Yasaei *et al.*[34] reported the influence of graphene grain boundaries on gas-sensing properties of graphene. They showed that the grain boundaries

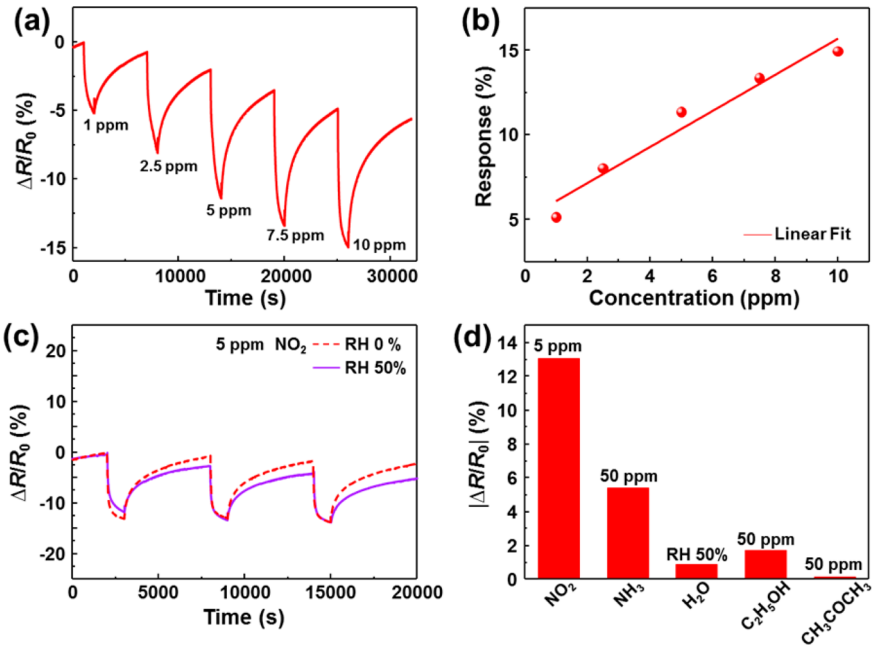

Figure 4. (a) Response curves to different NO_2 concentrations at 60 V. (b) Linear fit of the responses as a function of NO_2 concentration at 60 V. (c) Response curves upon exposure to NO_2 5 ppm in 0% and 50% of relative humidity atmosphere at 60 V. (d) Responses of the all graphene sensor to 5 ppm of NO_2, 50% wet air, 50 ppm ammonia, ethanol, and acetone at room temperature 60 V.

acting as dominant gas adsorption sites in polycrystalline graphene have higher resistances and ~300 times higher sensitivity than a single-crystalline graphene grain. When the voltage is applied to the patterned sensor, voltage drop occurs mainly in the narrow channel. Since the CVD graphene is polycrystalline, the narrow channel is a series connection of graphene grains and grain boundaries. As a result, voltage drop across the grain boundaries is much larger than that through the grains. Therefore, Joule heating could be predominant in the grain boundaries, which are attributed to the local heating spots in the patterned all graphene sensor. Further studies are needed to investigate the influence of graphene grain boundaries for adsorption and desorption of gas molecules in our graphene sensors.

To evaluate the detection limit of the patterned graphene sensor to NO_2 under the self-activated state, the response of the sensor was measured to 1−10 ppm of NO_2 as shown in Figure 4a. The $\Delta R/R_0$ values proportionally increases with increasing the NO_2 concentration. The base resistance is shifting with increasing the NO_2 concentration because the longer time is required for full recovery. The response values were plotted as a function of the gas concentration in Figure 4b. A simple linear regression fit was applied to find the linear relationship between the responses and the concentrations. The linear regression equation is expressed as $y = 1.067x + 5.01$, where y is the response and x is the concentration of NO_2. The measure of goodness-of-fit of the linear regression, r^2, was calculated to be 0.943. The responses of the sensor are 5.13, 8.04, 11.35, 13.36, and 14.94 to 1, 2.5, 5, 7.5, and 10 ppm of NO_2. Although the NO_2 concentration of 1 ppm was the lowest examined experimentally in the present study, the theoretical detection limit was calculated to be approximately 6.87 parts per billion (ppb)[35,36] (see the Supporting Information for details). This subppb level of the detection limits to NO_2 suggests its potential for use in various applications such as environmental monitoring and breath analysis, especially for diagnosing asthma. For the practical use of chemoresistive sensors in various applications, the water vapor poisoning effect has to be overcome. Typically, chemoresistive sensing properties of gas sensors based on semiconducting metal oxides are deteriorated in humidity condition.[37,38] We have measured dynamic sensing transients of the patterned graphene sensor to 5 ppm of NO_2 in dry (0% relative humidity) and humid (50% relative humidity) atmosphere (Figure 4c). Although the sensing properties were slightly deteriorated in terms of response and recovery, the degradation was less than ~5% in the humidity condition, which has not been reported for graphene-based gas sensors. It is noted that the degradation level is much lower than those of semiconducting metal oxide gas sensors which were depicted in previous works.[39,40] This result suggests that the self-activation plays a role in reducing the humidity effect.

Figure 4d shows responses ($|\Delta R/R_0|$) of the patterned all-graphene sensor to 5 ppm of NO_2, 50 ppm of NH_3, 50% relative humidity air, 50 ppm of C_2H_5OH, and 50 ppm of CH_3COCH_3 at the applied voltage of 60 V. Even the NO_2 concentration is the lowest as at 5 ppm

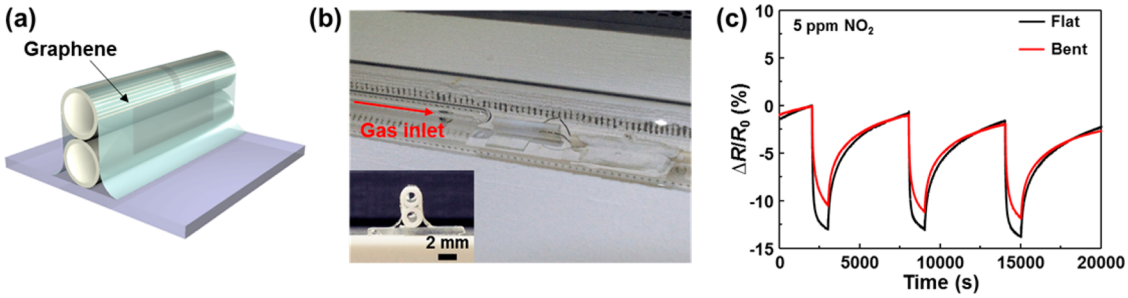

Figure 5. (a) Schematic for the patterned all-graphene sensor attached on ball pen leads. (b) Optical image of the gas sensing setup for the sensor under bending strain. The inset shows a side-view photograph of the sensor bent with a bending radius of 1 mm. (c) Response curves of the sensor without and with the bending strain.

the sensor shows the highest response to NO_2 (~13%). The responses to 50 ppm of NH_3, C_2H_5OH, CH_3COCH_3, and 50% RH air are 5.4, 1.71, 0.17, and 0.9%, respectively. The dynamic sensing transients to each gas are displayed in Supplementary Figure S3. This result demonstrates the high selectivity of the all-graphene sensor to NO_2.

The sensing performance with high bending strain was also investigated, which broadens the applications of the possibility of the self-activated all-graphene gas sensor applications to wearable electronics. To validate stable sensing operation under bending strain, the patterned graphene sensor was attached on two ball pen leads (bending radius of 1 mm). The bent sensor was fixed on a glass substrate and then was loaded to the chamber of the gas sensing measurement system (Figures 5a,b; see Supplementary Figure S4 for detailed photographs of the bent sensor). Figure 5c shows the sensing curves of the all graphene sensor without and with the bending strain (flat and bent). When the sensor was bent, the sensor still worked owing to the high flexibility of the graphene.[41] It is known that the resistance of graphene is increased by mechanical bending strain.[42,43] As a result, the lowered current density in the micropatterned graphene channel can weaken the self-activation that influences the sensing response. Despite this, the bent sensor shows only ~3% degradation in the response compared with the flat sensor. To our best knowledge, no one has shown gas sensors working under such a high bending strain (bending radius of 1 mm).

In addition to resistance to humidity conditions and stability over long-term operation, low power consumption is required for practical applications of the all-graphene sensor as a component in hand-held IoT devices such as mobile phones, smart watches, and tablet personal computers. To handle this issue, we have measured the power consumption of the sensor. By increasing the applied voltage from 1 to 60 V, the power consumption increases from 12 μW to 14.2 mW (Supplementary Figure S5). These values are comparable or even lower than the power consumption of micromachined thin film chemoresistive sensors (5−200 mW).[44,45] We believe that lower power consumption of the self-activated all graphene sensors can be obtained by nanostructuring or functionalizing the graphene channel and making the narrow channel free-standing, which enables the self-activation with reduced voltages or currents. Since the fabrication process of the all graphene sensors is very simple, this superior performance of the all graphene sensor demonstrates the feasibility of embedding them into portable and wearable devices.

CONCLUSION

We have developed the self-activated all-graphene NO_2 sensors with high transparency, flexibility, and low power consumption. The all-graphene sensor showed self-activation by increasing the bias voltage and the consequent enhancement of gas sensing properties such as fast response and reversible sensing behavior without external heating. The reliable room-temperature operation guarantees the stability of graphene sensing layer which could be distorted and eliminated by high-temperature operation.[46] Moreover, the sensor composed of single material, graphene, enables an entirely transparent and flexible device structure leading to reliable sensing performances under extremely high bending strain. We believe that the remarkable device performance, achieved with a simple fabrication process, significantly enlarges the potential of gas sensor applications to the next-generation technologies, such as the IoT and wearable electronics.

EXPERIMENTAL SECTION

Graphene Synthesis: Multiple Stacking Process. Graphene was synthesized on a Cu foil (purity: 99.99%) using a thermal chemical vapor deposition method at 1000 °C with hydrocarbon source (CH_4, 30 sccm) and hydrogen (H_2, 3 sccm). After one side of the as-synthesized sample was coated with PMMA, the graphene on the other side was removed by oxygen plasma using the reactive ion etcher. The Cu foil was etched with ammonium persulfate solution, and the graphene was subsequently rinsed with distilled water. The floating graphene was transferred on another as-synthesized sample to fabricate

multilayered graphene. Finally, the PMMA supporting polymer on the graphene was removed by acetone treatment.

Graphene Patterning and Transferring Process. 3LG on the Cu foil was patterned by photolithography and O_2 plasma treatment (6 s) with 50 W plasma power. An additional PMMA layer was coated on top of the patterned graphene to transfer the sample on a desired substrate. The patterned graphene with polymer was transferred on a transparent PI film, and the sample was soaked in acetone to remove the supporting polymer (PMMA and PR) layers.

Sensor Measurements. The gas-sensing properties of the fabricated graphene sensors were measured without external heating. As the flow gas was changed from dry air to a calibrated test gas (balanced with dry air, Sinjin Gases), the variation in sensor resistance was monitored using a source measurement unit (Keithley 2365B). A constant flow rate of 1000 sccm was used for dry air and the test gas. The sensor resistance was measured under a DC bias voltage of 1−60 V. The response of the sensors ($\Delta R/R_0$) was accurately determined by measuring the baseline resistances of the sensors in dry air and the fully saturated resistances after exposure to the test gas. Gas flow was controlled using mass flow controllers, and all measurements were recorded to a computer over a GPIB interface. The current−voltage characteristics of the fabricated sensors were measured to check the contribution of the contact resistance to the overall performance.

Conflict of Interest: The authors declare no competing financial interest.

Supporting Information Available: The Supporting Information is available free of charge on the ACS Publications website at DOI: 10.1021/acsnano.5b04680.

Additional information and figures (PDF)

Acknowledgment. This work was financially supported by the Center for Integrated Smart Sensors funded by the Ministry of Science, ICT & Future Planning as the Global Frontier Project, the Outstanding Young Researcher Program, and the Fusion Research Program for Green Technologies through the National Research Foundation of Korea.

REFERENCES AND NOTES

1. Swan, M. Sensor Mania! The Internet of Things, Wearable Computing, Objective Metrics, and the Quantified Self 2.0. *J. Sens. Actuator Networks* **2012**, *1*, 217–253.
2. Miorandi, D.; Sicari, S.; De Pellegrini, F.; Chlamtac, I. Internet of Things: Vision, Applications and Research Challenges. *Ad Hoc Netw.* **2012**, *10*, 1497–1516.
3. Barsan, N.; Koziej, D.; Weimar, U. Metal Oxide-Based Gas Sensor Research: How to? *Sens. Actuators, B* **2007**, *121*, 18–35.
4. Nanto, H.; Sokooshi, H.; Kawai, T. Aluminum-Doped ZnO Thin Film Gas Sensor Capable of Detecting Freshness of Sea Foods. *Sens. Actuators, B* **1993**, *14*, 715–717.
5. Yamazoe, N. Toward Innovations of Gas Sensor Technology. *Sens. Actuators, B* **2005**, *108*, 2–14.
6. Moos, R.; Müller, R.; Plog, C.; Knezevic, A.; Leye, H.; Irion, E.; Braun, T.; Marquardt, K.-J.; Binder, K. Selective Ammonia Exhaust Gas Sensor for Automotive Applications. *Sens. Actuators, B* **2002**, *83*, 181–189.
7. Capone, S.; Forleo, A.; Francioso, L.; Rella, R.; Siciliano, P.; Spadavecchia, J.; Presicce, D.; Taurino, A. Solid State Gas Sensors: State of the Art and Future Activities. *J. Optoelectron.: Adv. Mater. Devices* **2003**, *5*, 1335–1348.
8. Yamazoe, N.; Shimanoe, K. New Perspectives of Gas Sensor Technology. *Sens. Actuators, B* **2009**, *138*, 100–107.
9. Moon, H. G.; Shim, Y.-S.; Kim, D. H.; Jeong, H. Y.; Jeong, M.; Jung, J. Y.; Han, S. M.; Kim, J. K.; Kim, J.-S.; Park, H.-H. Self-Activated Ultrahigh Chemosensitivity of Oxide Thin Film Nanostructures for Transparent Sensors. *Sci. Rep.* **2012**, *2*, 588.
10. Yamazoe, N. New Approaches for Improving Semiconductor Gas Sensors. *Sens. Actuators, B* **1991**, *5*, 7–19.
11. Eranna, G.; Joshi, B.; Runthala, D.; Gupta, R. Oxide Materials for Development of Integrated Gas Sensors—A Comprehensive Review. *Crit. Rev. Solid State Mater. Sci.* **2004**, *29*, 111–188.
12. Schedin, F.; Geim, A.; Morozov, S.; Hill, E.; Blake, P.; Katsnelson, M.; Novoselov, K. Detection of Individual Gas Molecules Adsorbed on Graphene. *Nat. Mater.* **2007**, *6*, 652–655.
13. Lu, G.; Park, S.; Yu, K.; Ruoff, R. S.; Ocola, L. E.; Rosenmann, D.; Chen, J. Toward Practical Gas Sensing with Highly Reduced Graphene Oxide: A New Signal Processing Method to Circumvent Run-to-Run and Device-to-Device Variations. *ACS Nano* **2011**, *5*, 1154–1164.
14. Dan, Y.; Lu, Y.; Kybert, N. J.; Luo, Z.; Johnson, A. C. Intrinsic Response of Graphene Vapor Sensors. *Nano Lett.* **2009**, *9*, 1472–1475.
15. Robinson, J. T.; Perkins, F. K.; Snow, E. S.; Wei, Z.; Sheehan, P. E. Reduced Graphene Oxide Molecular Sensors. *Nano Lett.* **2008**, *8*, 3137–3140.
16. Fowler, J. D.; Allen, M. J.; Tung, V. C.; Yang, Y.; Kaner, R. B.; Weiller, B. H. Practical Chemical Sensors from Chemically Derived Graphene. *ACS Nano* **2009**, *3*, 301–306.
17. Lu, G.; Ocola, L. E.; Chen, J. Gas Detection Using Low-Temperature Reduced Graphene Oxide Sheets. *Appl. Phys. Lett.* **2009**, *94*, 083111.
18. He, Q.; Sudibya, H. G.; Yin, Z.; Wu, S.; Li, H.; Boey, F.; Huang, W.; Chen, P.; Zhang, H. Centimeter-Long and Large-Scale Micropatterns of Reduced Graphene Oxide Films: Fabrication and Sensing Applications. *ACS Nano* **2010**, *4*, 3201–3208.
19. Lipatov, A.; Varezhnikov, A.; Wilson, P.; Sysoev, V.; Kolmakov, A.; Sinitskii, A. Highly Selective Gas Sensor Arrays Based on Thermally Reduced Graphene Oxide. *Nanoscale* **2013**, *5*, 5426–5434.
20. Cui, S.; Pu, H.; Mattson, E. C.; Wen, Z.; Chang, J.; Hou, Y.; Hirschmugl, C. J.; Chen, J. Ultrasensitive Chemical Sensing through Facile Tuning Defects and Functional Groups in Reduced Graphene Oxide. *Anal. Chem.* **2014**, *86*, 7516–7522.
21. Li, W.; Geng, X.; Guo, Y.; Rong, J.; Gong, Y.; Wu, L.; Zhang, X.; Li, P.; Xu, J.; Cheng, G. Reduced Graphene Oxide Electrically Contacted Graphene Sensor for Highly Sensitive Nitric Oxide Detection. *ACS Nano* **2011**, *5*, 6955–6961.
22. Nomani, M. W.; Shishir, R.; Qazi, M.; Diwan, D.; Shields, V.; Spencer, M.; Tompa, G. S.; Sbrockey, N. M.; Koley, G. Highly Sensitive and Selective Detection of NO_2 Using Epitaxial Graphene on 6H-SiC. *Sens. Actuators, B* **2010**, *150*, 301–307.
23. Yu, K.; Wang, P.; Lu, G.; Chen, K.-H.; Bo, Z.; Chen, J. Patterning Vertically Oriented Graphene Sheets for Nanodevice Applications. *J. Phys. Chem. Lett.* **2011**, *2*, 537–542.
24. Dai, J.; Giannozzi, P.; Yuan, J. Adsorption of Pairs of NO_x Molecules on Single-Walled Carbon Nanotubes and Formation of NO + NO_3 from NO_2. *Surf. Sci.* **2009**, *603*, 3234–3238.
25. Ueda, T.; Bhuiyan, M.; Norimatsu, H.; Katsuki, S.; Ikegami, T.; Mitsugi, F. Development of Carbon Nanotube-Based Gas Sensors for NO_x Gas Detection Working at Low Temperature. *Phys. E* **2008**, *40*, 2272–2277.
26. Choi, H.; Choi, J. S.; Kim, J. S.; Choe, J. H.; Chung, K. H.; Shin, J. W.; Kim, J. T.; Youn, D. H.; Kim, K. C.; Lee, J. I. Flexible and Transparent Gas Molecule Sensor Integrated with Sensing and Heating Graphene Layers. *Small* **2014**, *10*, 3685–3691.
27. Sui, D.; Huang, Y.; Huang, L.; Liang, J.; Ma, Y.; Chen, Y. Flexible and Transparent Electrothermal Film Heaters Based on Graphene Materials. *Small* **2011**, *7*, 3186–3192.
28. Cançado, L. G.; Jorio, A.; Ferreira, E. M.; Stavale, F.; Achete, C.; Capaz, R.; Moutinho, M.; Lombardo, A.; Kulmala, T.; Ferrari, A. Quantifying Defects in Graphene *via* Raman Spectroscopy at Different Excitation Energies. *Nano Lett.* **2011**, *11*, 3190–3196.
29. Kumar, B.; Min, K.; Bashirzadeh, M.; Farimani, A. B.; Bae, M.-H.; Estrada, D.; Kim, Y.; Yasaei, P.; Park, Y.; Pop, E. The Role of External Defects in Chemical Sensing of Graphene Field-Effect Transistors. *Nano Lett.* **2013**, *13*, 1962–1968.
30. Yavari, F.; Chen, Z.; Thomas, A. V.; Ren, W.; Cheng, H.-M.; Koratkar, N. High Sensitivity Gas Detection Using a Macroscopic Three-Dimensional Graphene Foam Network. *Sci. Rep.* **2011**, *1*, 166.
31. Jeong, H. Y.; Lee, D.-S.; Choi, H. K.; Lee, D. H.; Kim, J.-E.; Lee, J. Y.; Lee, W. J.; Kim, S. O.; Choi, S.-Y. Flexible

Room-Temperature NO_2 Gas Sensors Based on Carbon Nanotubes/Reduced Graphene Hybrid Films. *Appl. Phys. Lett.* **2010**, *96*, 213105.
32. Chung, M. G.; Kim, D. H.; Lee, H. M.; Kim, T.; Choi, J. H.; kyun Seo, D.; Yoo, J.-B.; Hong, S.-H.; Kang, T. J.; Kim, Y. H. Highly Sensitive NO_2 Gas Sensor Based on Ozone Treated Graphene. *Sens. Actuators, B* **2012**, *166*, 172–176.
33. Karaduman, I.; Er, E.; Çelikkan, H.; Acar, S. A New Generation Gas Sensing Material Based on High-Quality Graphene. *Sens. Actuators, B* **2015**, *221*, 1188–1194.
34. Yasaei, P.; Kumar, B.; Hantehzadeh, R.; Kayyalha, M.; Baskin, A.; Repnin, N.; Wang, C.; Klie, R. F.; Chen, Y. P.; Král, P. Chemical Sensing with Switchable Transport Channels in Graphene Grain Boundaries. *Nat. Commun.* **2014**, *5*, 4911.
35. Dua, V.; Surwade, S. P.; Ammu, S.; Agnihotra, S. R.; Jain, S.; Roberts, K. E.; Park, S.; Ruoff, R. S.; Manohar, S. K. All-Organic Vapor Sensor Using Inkjet-Printed Reduced Graphene Oxide. *Angew. Chem., Int. Ed.* **2010**, *49*, 2154–2157.
36. Li, J.; Lu, Y.; Ye, Q.; Cinke, M.; Han, J.; Meyyappan, M. Carbon Nanotube Sensors for Gas and Organic Vapor Detection. *Nano Lett.* **2003**, *3*, 929–933.
37. Koziej, D.; Bârsan, N.; Weimar, U.; Szuber, J.; Shimanoe, K.; Yamazoe, N. Water−Oxygen Interplay on Tin Dioxide Surface: Implication on Gas Sensing. *Chem. Phys. Lett.* **2005**, *410*, 321–323.
38. Vlachos, D.; Skafidas, P.; Avaritsiotis, J. The Effect of Humidity on Tin-Oxide Thick-Film Gas Sensors in the Presence of Reducing and Combustible Gases. *Sens. Actuators, B* **1995**, *25*, 491–494.
39. Dieguez, A.; Vila, A.; Cabot, A.; Romano-Rodrguez, A.; Morante, J.; Kappler, J.; Barsan, N.; Weimar, U.; Göpel, W. Influence on the Gas Sensor Performances of the Metal Chemical States Introduced by Impregnation of Calcinated SnO_2 Sol−Gel Nanocrystals. *Sens. Actuators, B* **2000**, *68*, 94–99.
40. Neri, G.; Bonavita, A.; Galvagno, S.; Siciliano, P.; Capone, S. CO and NO_2 Sensing Properties of Doped-Fe_2O_3 Thin Films Prepared by LPD. *Sens. Actuators, B* **2002**, *82*, 40–47.
41. Bae, S.; Kim, H.; Lee, Y.; Xu, X.; Park, J.-S.; Zheng, Y.; Balakrishnan, J.; Lei, T.; Kim, H. R.; Song, Y. I. Roll-to-Roll Production of 30-Inch Graphene Films for Transparent Electrodes. *Nat. Nanotechnol.* **2010**, *5*, 574–578.
42. Kim, K. S.; Zhao, Y.; Jang, H.; Lee, S. Y.; Kim, J. M.; Kim, K. S.; Ahn, J.-H.; Kim, P.; Choi, J.-Y.; Hong, B. H. Large-Scale Pattern Growth of Graphene Films for Stretchable Transparent Electrodes. *Nature* **2009**, *457*, 706–710.
43. Li, X.; Zhu, Y.; Cai, W.; Borysiak, M.; Han, B.; Chen, D.; Piner, R. D.; Colombo, L.; Ruoff, R. S. Transfer of Large-Area Graphene Films for High-Performance Transparent Conductive Electrodes. *Nano Lett.* **2009**, *9*, 4359–4363.
44. Simon, I.; Bârsan, N.; Bauer, M.; Weimar, U. Micromachined Metal Oxide Gas Sensors: Opportunities to Improve Sensor Performance. *Sens. Actuators, B* **2001**, *73*, 1–26.
45. Elmi, I.; Zampolli, S.; Cozzani, E.; Mancarella, F.; Cardinali, G. Development of Ultra-Low-Power Consumption MOX Sensors with Ppb-Level VOC Detection Capabilities for Emerging Applications. *Sens. Actuators, B* **2008**, *135*, 342–351.
46. Radovic, L. R. Active Sites in Graphene and the Mechanism of CO_2 Formation in Carbon Oxidation. *J. Am. Chem. Soc.* **2009**, *131*, 17166–17175.